Insight into the Liquid Structure of Water and Sodium Chloride Solutions Using Stimulated Raman Scattering

Zhixin Wu,[1,2] Zhengping Wang,[1,2,*] Xun Sun,[1,2] Lisong Zhang,[1,2] Mingxia Xu,[1,2] and Xinguang Xu[1,2]

[1] *State Key Laboratory of Crystal Materials, Shandong University, Jinan, 250100, China*

[2] *Key Laboratory of Functional Crystal Materials and Device (Shandong University), Ministry of Education, Jinan, 250100, China*

(Received 20 January 2019; revised manuscript received 1 December 2019; accepted 9 January 2020; published 12 February 2020)

By dissolving sodium chloride (NaCl) in liquid water, we realize an obvious enhancement of stimulated Raman scattering (SRS). Compared with pure water, the performance improvements include spectrum purification, an increased Raman gain, a decreased pump threshold, and an increased conversion efficiency. In the best SRS results, the pump threshold decreases by 45% and the maximum conversion efficiency increases by 10.4%. Then, water becomes a typical Raman-scattering medium that generates narrowband light. Moreover, we find that the bulk structure of water and NaCl solutions can be analyzed in detail by combining the principles of SRS and analysis of the SRS spectra. In water, the O—H stretching band is proved to be a superposition of stretching modes of different water clusters. For the solution, the O—H stretching vibration of water molecules in hydration shells around Cl^- ions can be obtained directly, and its variation with respect to solute concentration is investigated using SRS spectra. The superior SRS properties of solutions originate from the hydration shell around the Cl^- ions. This work suggests that SRS is a promising approach to identifying structures in water and NaCl solutions, and that it can easily be extended to other liquids and solutions.

DOI: 10.1103/PhysRevApplied.13.024030

I. INTRODUCTION

The structure of liquid water and aqueous solutions of inorganic salts has been of great interest because of its role in reaction chemistry, nutrition, biochemistry, and biology, amongst other things [1–3]. A number of theoretical and experimental studies have been performed on intermolecular motion in water and ion-water interactions in solutions [4–13]. Microscopic information, including information about hydrogen-bond structures, ion pairs, hydration, O—H stretching bands, and higher-order water clusters, has been analyzed using thermodynamics, neutron and x-ray diffraction, dynamic light scattering, zeta-potential measurements, IR absorption, and Raman spectroscopy [4–8]. Besides experimental studies, computer simulations based on classical molecular dynamics, Monte Carlo simulations, and combined quantum mechanical and molecular dynamics simulations have been used to describe the interactions of particles [9–13].

However, the hydrogen-bonding network environment in liquid water and the mechanism of the perturbing effect of ions are still unclear. Different have been models were introduced to interpret the observable properties of water, including atomically detailed semiempirical models, fixed-charge models, polarizable models, and a mixture of structure types [14]. At the same time, many research projects have shown that ions dissolved in liquid water can be classified as "structure makers" or "structure breakers" [15,16]. In spite of this, results obtained from femtosecond pump-probe spectroscopy have shown that ions do not lead to any enhancement or breakdown of the hydrogen-bond network in water [17]. Lately, some techniques and methods have been applied to analyze the structure of the liquid. The long-range behavior of water and salt water was investigated using polarization-resolved second-harmonic scattering operated in a right-angle configuration [18]. Images of Na^+ hydrates (Na^+ nD_2O, $n = 1$–5) were obtained using a combined noncontact atomic force microscopy and scanning tunnelling microscopy system at 5 K [19]. Although this provided a method to study various hydration processes at the atomic scale, the exploration of the bulk structure of a solution at normal temperature still faces problems.

Spontaneous Raman scattering is an important technology used to investigate the intra- and intermolecular vibrational modes of water and solutions. Through the use of spontaneous-Raman-scattering measurements, the influence of various factors on the structure of water, such as temperature [20,21], pressure [22], and the presence of ions [23–25], can be explored. Nevertheless, the

*zpwang@sdu.edu.cn

spontaneous-Raman-scattering spectrum is broadband, and the corresponding structural analysis has poor resolution, which makes spectral assignment difficult. When a Raman medium is pumped by a strong laser beam, the spontaneous Raman scattering may serve as the signal light, and develop into a strong stimulated-Raman-scattering (SRS) output through energy transfer from the pump light [26–28]. In recent years, SRS technology has been increasingly applied to investigate physical phenomena in liquid water under intense light fields, such as laser-induced breakdown, laser-induced shock compression, and hydrated-electron resonance [29–34].

In the work presented in this paper, SRS technology is applied to analyze the bulk structure of water and sodium chloride (NaCl) solutions. Through SRS spectra, liquid water is proved be an assemblage of different clusters which can be quantified. In NaCl solutions, large water clusters with strong hydrogen bonds are destroyed and hydration shells are formed. The SRS spectra clearly display the stretching vibration modes of water clusters in the hydration shells around Cl^- ions, as well as their blueshifts with an increase in NaCl concentration. Compared with differential Raman spectroscopy and the Raman ratio spectrum, the SRS technology reported here is more intuitive. These results will be of great importance to further research on the structure and structure-property relationships of water and solutions.

Besides, from the application point of view, by utilizing the enhancement of the main peak cross section obtained by dissolving NaCl [25,35], we realized an obvious improvement in the SRS performance of liquid water. As a nonelastic third-order nonlinear optical (NLO) effect, SRS has been used as one of the most efficient optical frequency-conversion technologies [36–38], while for water, because it has a lower Raman gain coefficient than other liquids, its SRS effect is seldom applied in practical NLO frequency conversion, although it is the most common liquid in the world. Previously, several different methods have been attempted to solve this problem, including cooling [39], focusing [40,41], and pumping with stimulated Brillouin scattering [42]. Our research confirms that the SRS properties of water can be obviously enhanced by dissolving a solid inorganic compound, such as sodium chloride, as reported here. The pump threshold can be decreased by 45%, and the maximum conversion efficiency can be increased by 10.4%. This method offers the possibility of helping SRS in water to achieve more applications, and at the same time it can be extended to other liquids to achieve better SRS characteristics. So, we consider it to be a very important piece of technical progress, which is simple, efficient, low cost, and reliable.

II. EXPERIMENTAL SETUP FOR STIMULATED RAMAN SCATTERING

In our experiment, deionized water and a series of aqueous NaCl solutions of varying concentrations are prepared for spontaneous-Raman-spectroscopy measurements (see the Supplemental Material [43], Sec. I) and SRS experiments. The conductivity of the deionized water used in this work is 5.8×10^{-6} S·m^{-1}, and the analytical-reagent grade of the NaCl is 99.5% purity. All the experiments are performed at 293 ± 1 K.

In general, forward SRS (FSRS) and backward SRS appear simultaneously in SRS experiments [53,54]. We focus the forward SRS of water and the NaCl solutions, because the signal of backward SRS is usually faint and it mixes with forward SRS reflected by optical components. A schematic diagram of the experimental setup for measuring FSRS spectra and energies in water and NaCl aqueous solutions is shown in Fig. 1. A dye mode-locked neodymium-doped yttrium aluminum garnet laser (PY61C-10, Continuum Inc., USA), producing a single longitudinal-mode 1064-nm beam with a pulse duration of 40 ps at a repetition rate of 10 Hz, is used as the fundamental light source. This can provide a high-peak-power-density laser with low energy. So, thermal effects during SRS generation can be reduced effectively. A shaping diaphragm (F) with a diameter of 6 mm intercepts the fundamental laser beam to improve the beam quality. A KTP crystal is used as a frequency doubler to generate the 532-nm pump laser. The pulse duration of the 532-nm pump laser is measured to be 35 ps. The coated mirror M1 is highly reflective at 1064 nm and highly transmissive at 532 nm, and serves as a filter for the fundamental laser. An $f = 1200$ mm planoconvex lens (L1) is used to focus the

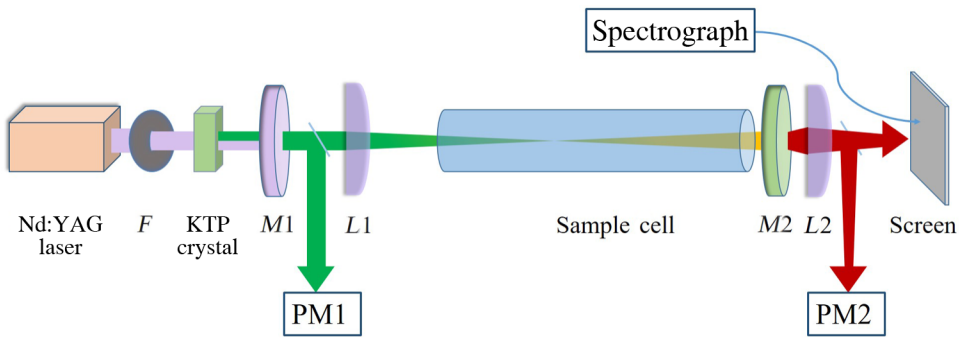

FIG. 1. Schematic diagram of the experimental setup.

532-nm laser beam into a sample cell of length 500 mm equipped with fused-silica optical windows. In order to avoid damaging the cell windows and to increase the pump pulse energy, L1 is placed 45 cm from the front window of the cell. In order to measure the SRS spectra and output energy, a mirror (M2) is used to filter out the residual 532-nm pump laser. The divergent SRS beam is collected by an $f = 50$ mm planoconvex lens (L2). The energies of the pump laser and SRS laser are measured using two beam splitters and two power meters (PM1 and PM2). The SRS spectrum is collected from the receiving screen with an optical-fiber-coupled spectrometer (HR4000CG-UV-NIR, Ocean Optics Inc.).

III. EXPERIMENTAL RESULTS ON STIMULATED RAMAN SCATTERING

Firstly, the pump thresholds for SRS are measured under identical conditions for pure water and NaCl aqueous solutions of varying concentrations. Here, the threshold is defined as the minimum energy for which our experimental apparatus can reveal a signal. The main technical specifications of the pyroelectric energy sensor used (ES111C, THORLABS) include a wavelength range of 0.185–25 μm, an energy range of 10 μJ–150 mJ, and a resolution of 100 nJ. From Fig. 2, it can be seen that the highest threshold is associated with pure water. In addition, an increase in the NaCl content corresponds to the SRS threshold demonstrating a decreasing trend. Comparing the first Stokes spectral line near the pump threshold between water and the solutions (see the Supplemental Material [43], Sec. II), this phenomenon can be attributed to suppression of the shoulder peak in the NaCl solutions and the pump energy being concentrated on exciting the main peak.

For further evaluation of the enhancement of SRS through the use of dissolved NaCl, the Raman gain of pure water and NaCl solutions of varying concentrations is investigated. With the spontaneous Raman linewidth $\Delta\Omega_R$ measured, as shown in Fig. S1 (see the Supplemental Material [43], Sec. I), the Raman gain of water can be calculated as 0.27 cm/GW [55,56]. The phonon relaxation time $T_R = (\pi c\,\Delta\Omega_R)^{-1}$ is 0.1 ps, which completely fulfills the steady-state SRS condition $\tau_p \gg T_R$. Here c is the speed of light in vacuum, and τ_p is the full width at half maximum of the 532-nm pump pulse, which is 35 ps in this experiment. In this situation, the Raman gain g_R of the NaCl solutions can be calculated based on the following relationship between the threshold and the gain [57]:

$$g_R I_{\mathrm{thr}} l_{\mathrm{SRS}} = 25, \tag{1}$$

where I_{thr} is the pump laser intensity at the threshold of the first Stokes line, and l_{SRS} is the length of the sample cell. The Raman gains of the NaCl solutions are calculated as 0.32, 0.38, 0.42, and 0.49 cm/GW for concentrations of 1.63, 2.72, 4.07, and 5.43 mol·l^{-1}, respectively. It is clear that the Raman gain increases with concentration, as shown in Fig. 2.

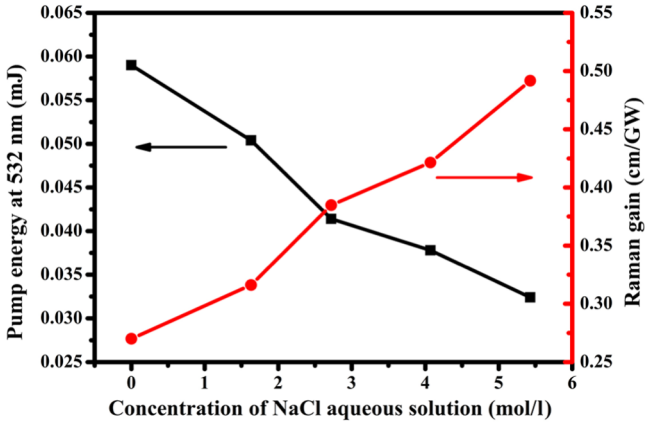

FIG. 2. SRS threshold pump energy for water and NaCl aqueous solutions of varying concentrations.

The first-Stokes output characteristics are also recorded in a pump range of 0–1.53 mJ for varying pump energies at 532 nm, as shown in Fig. 3. Below 0.5 mJ, the conversion efficiency from pump energy to SRS energy increases rapidly both in water and in the solutions. Above 0.5 mJ, the efficiency in water is maintained at approximately 35%, reaching a maximum value of 37.1%. For the solutions, there is an interval during which the efficiency is greater than that observed in water. This interval and the maximum efficiency increase for concentrations that vary from 1.63 to 4.07 mol·l^{-1}. The maximum interval (0–1.5 mJ) and efficiency (44.2%) are achieved for a NaCl solution with a concentration of 4.07 mol·l^{-1}. At a pump energy of 0.81 mJ, the absolute SRS efficiency is 10.4% greater than that of water, corresponding to a 30.8% enhancement. The declining conversion efficiency at higher energies is due to the enhancement of diffuse scattering in the solutions. The maximum efficiency of the 5.43 mol·l^{-1} NaCl solution does not exceed the value achieved for the 4.07 mol·l^{-1} sample, because of the obvious scattering effect in the saturated solution.

It should be noted that during the process of our experiment no supercontinuum-generation (SC) phenomenon is observed by monitoring the spectral profile and laser color of the output beam. Previously, De Boni *et al.* reported SC generation in water with a picosecond Nd:YAG laser as the pump source [58]. In that work, the pump threshold for SC generation was about 4 mJ, corresponding to a power density of 1.2×10^{12} W/cm^2. In our experiment, the maximum pump energy is 1.53 mJ, corresponding to a power density of 3×10^{11} W/cm^2. From this, we speculate that the main reason for not observing SC generation here is that the energy range we use is lower than the pump threshold for that process.

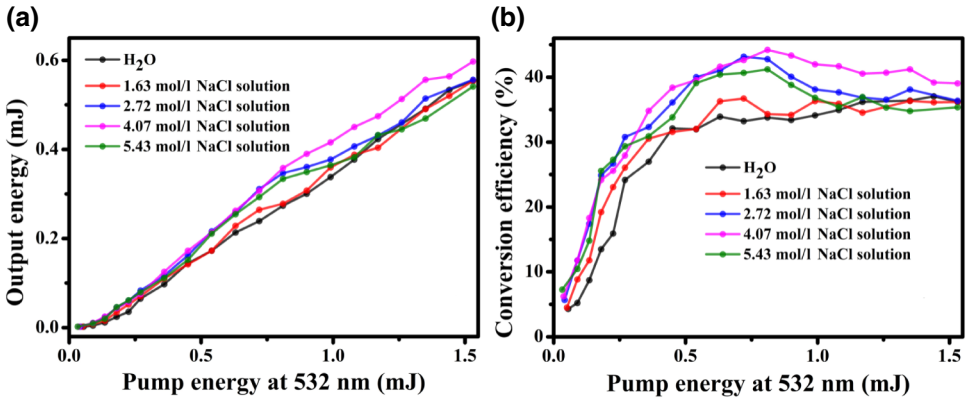

FIG. 3. (a) Stimulated-Raman-scattering energy and (b) optical conversion efficiency with respect to the pump energy at 532 nm for water and NaCl aqueous solutions of varying concentrations.

IV. DISCUSSION

The SRS spectra of water and the solutions are captured at the highest pump energy of 1.53 mJ in order to explore the reasons for the SRS enhancement phenomenon, as shown in Fig. 4(a). In the measured energy range, only the first Stokes component is excited. For water, there are two high peaks at 650.0 and 649.3 nm, as well as a broad peak covering a range of 640–655 nm corresponding to a Raman shift from 3100 to 3566 cm^{-1}. For the NaCl solutions, the shoulder peaks are suppressed, and the peak shapes are almost symmetric. The SRS peaks are close to a single-peak Gaussian distribution, as shown in Figs. 4(c)–4(f). So, it can be said that a spectral cleanup effect occurs when NaCl is dissolved in water. The spontaneous-Raman-scattering spectra also show the same effect (see Fig. S4 in the Supplemental Material [43], Sec. I). According to Eqs. (S3) and (S4) in the Supplemental Material [43], the SRS intensity I_s increases with the Raman gain coefficient g_R, while g_R is inversely proportional to the spontaneous Raman linewidth $\Delta\nu$. Therefore, the spectral cleanup effect (i.e., decreasing $\Delta\nu$) is favored for large g_R and a high SRS output. As a result, the NaCl solutions exhibit an obvious SRS enhancement relative to pure water.

As can be seen from Fig. S4 in the Supplemental Material [43], the SRS spectra have different shapes from the broadband spontaneous-Raman-scattering spectra. By analyzing the SRS spectra, the structures of water and the solutions can be explored in detail. For water, some small peaks in the SRS spectra become clear under strong excitation conditions. There are seven peaks that can be distinguished as being at 641.6, 642.4, 643.9, 645.5, 649.3, 650.0, and 654.1 nm. In Fig. 4(b), the SRS spectrum is deconvoluted into seven Gaussian subpeaks, and the fitted profile of the total signal basically agrees with the measured SRS spectrum. The Raman shifts of these subpeaks are 3213, 3232, 3262, 3308, 3398, 3416, and 3512 cm^{-1}, respectively. The seven first Stokes lines obtained in the experiment are incompatible with the five Gaussian components shown in FIG. S3 (see the Supplemental Material [43], Sec. I). It is expected that the O—H stretching band contains vibrational modes from different water clusters. As reported in Refs. [59–61], each cluster structure possesses its own O—H stretching vibrational modes. According to Eqs. (S3) and (S4) in the Supplemental Material [43], the vibrational modes with a high static Raman intensity are more likely to appear in the SRS spectrum, because of the large Raman gain. So, we compare the measured Raman shifts with the calculated modes reported in Ref. [61]. In Fig. 4(a), the two highest peaks for water are located at 3398 and 3416 cm^{-1}. They are close to the Raman frequencies of the tetramer, pentamer, and hexamer, i.e., 3396, 3442, and 3437 cm^{-1}, respectively [61]. Based on the principles of SRS generation (see the Supplemental Material [43], Sec. III), these water clusters are thus dominant in quantitative terms. As reported in Ref. [62], intracluster electron scattering is mainly determined by the short-range potential of clusters consisting of five or six molecules. This is consistent with our experiment results. It is interesting that some small peaks at low wave numbers are also excited by the intense laser. The Stokes lines at 3213, 3232, 3262, and 3308 cm^{-1} are derived from the larger water clusters, including the hexamer, heptamer, and octamer. They are similar to their Raman spectra at 3222, 3226, 3247, and 3348 cm^{-1}, respectively [61]. There is also a small peak at 3512 cm^{-1} in the SRS spectra. This Stokes line at high wave number is similar to the vibrational mode at 3524 cm^{-1} of the tetramer [61]. Although there may be errors in both the experimental measurements and the theoretical simulations, on the whole the deviations of the data are small (2–40 cm^{-1}). This indicates that the present assignment is solid, and that the SRS spectra can provide compelling evidence about the O—H stretching vibrations of H_2O molecules in different water clusters. Thus, the intensity $I(\nu)$ of the O—H stretching band can be expressed as

$$I(\nu) = I(\nu_1) + I(\nu_2) + I(\nu_3) + \cdots, \tag{2}$$

where $\nu_1, \nu_2, \nu_3, \ldots$ are the O—H stretching modes of the clusters. Based on the mechanism of SRS generation, the intensity $I(\nu_n)$ is linked to the quantity of the corresponding cluster involved in SRS generation (see the Supplemental

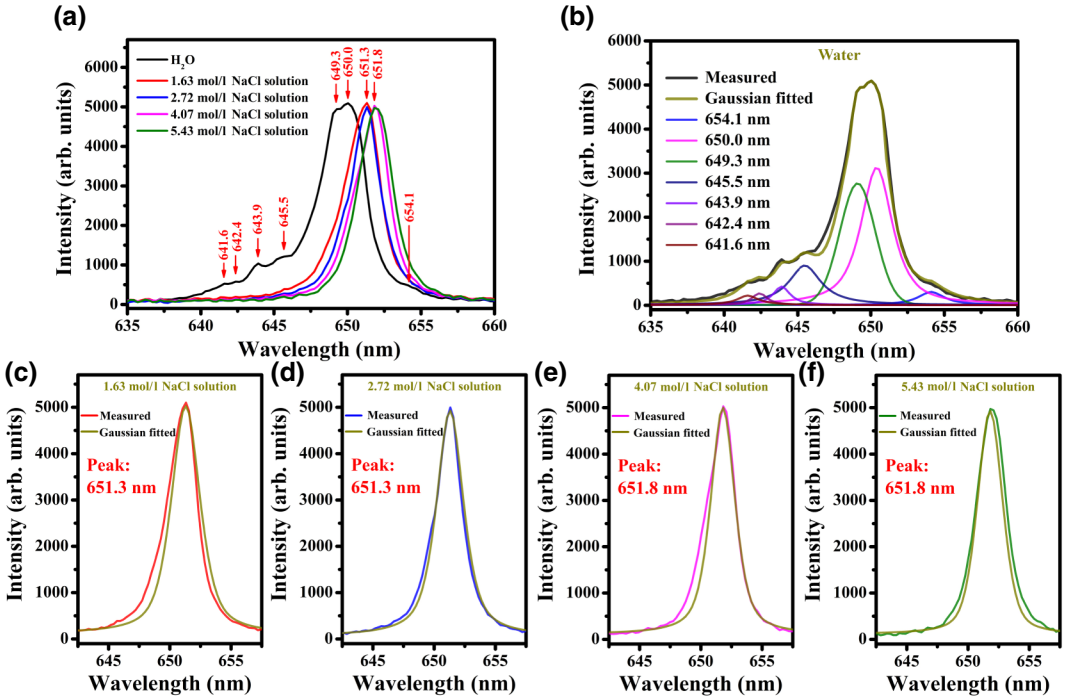

FIG. 4. SRS spectra and computer-deconvoluted Gaussian spectra of water and NaCl aqueous solutions of varying concentrations at a pump energy of 1.53 mJ. (a) Measured SRS spectra of water and NaCl aqueous solutions. (b)–(f) Computer-deconvoluted Gaussian spectra of water and NaCl solutions with concentrations of 1.63, 2.72, 4.07, and 5.43 mol·l^{-1}, respectively.

Material [43], Sec. III). The SRS spectra can thus provide a practical method for the statistical analysis and quantification of clusters in bulk water. The more water molecules present in a water cluster, the smaller the stretching frequency and the stronger the associated hydrogen bonds [59,61]. With this interpretation, simultaneously referencing Figs. 4(a) and 4(b) and Fig. S4 in the Supplemental Material [43], the conclusion can be drawn that large water clusters with strong hydrogen bonds are destroyed by the dissolution of NaCl. Compared with spontaneous-Raman-scattering spectra, a different insight into the liquid structure of water is presented.

In the SRS experiment, the Raman shifts are 3446, 3446, 3458, and 3458 cm^{-1} for NaCl solutions with concentrations of 1.63, 2.72, 4.07, and 5.43 mol l^{-1}, respectively. It is found that the Raman shifts in the NaCl solutions are close to the phonon wave numbers of the water molecules in the hydration shells around Cl^- ions centered at approximately 3450 cm^{-1} [35]. A schematic diagram of the aqueous solvation shells is plotted in Fig. 5. The water molecules surrounding the Na^+ ions participate in hydrogen bonding with other water molecules. In that regard, they are similar to bulk water. This phenomenon has been proved in a few research projects [25,63,64]. In the hydration shell of Cl^-, the H atoms in the water molecules are influenced directly by the electric field of the Cl^- ion. Thus, in the solution, the effect exerted by the Cl^- ions on the O—H stretching modes plays a major role. Then, we can conclude that the Raman shift in NaCl solutions originates from the O—H stretching vibrations of water molecules in the aqueous solvation shells of Cl^- ions.

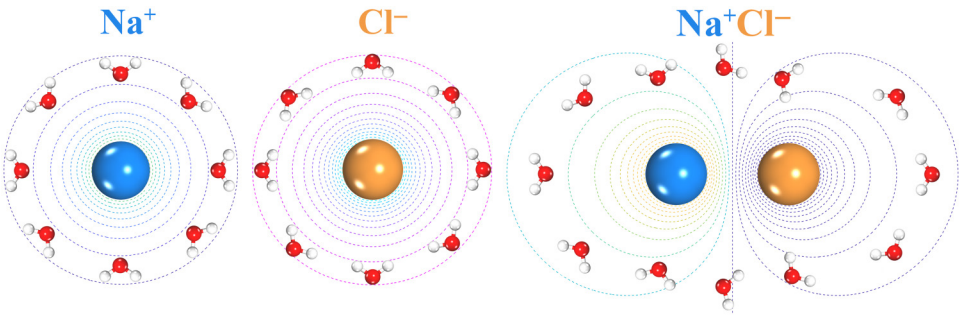

FIG. 5. Schematic diagram of aqueous solvation shells and the equipotential surfaces of Na^+, Cl^-, and a Na^+-Cl^- ion pair.

Based on the principles of SRS generation, the single symmetric SRS peak indicates that the water molecules in the hydration shell are dominant in the solution. While the numerical ratios of water molecules to Cl^- ions are 33/1, 19/1, 12/1, and 9/1 for solutions with concentrations of 1.63, 2.72, 4.07, and 5.43 mol l^{-1}, respectively, a maximum coordination number of 8.2 around Cl^- is achieved in dilute solutions according to molecular dynamics simulations [65]. The water molecules in the hydration shell in the 1.63 mol l^{-1} NaCl solution account for potentially the largest ratio, 8.2/33, of total water molecules. The low numerical proportion does not correspond to its dominating influence on the SRS generation. One reason is that the Raman-scattering cross section of water in a hydration shell is larger than that of bulk water [66]. Moreover, it is speculated that the other water molecules combine with the water molecules in the hydration shell through hydrogen bonding, and those molecules possess a similar stretching vibrational mode. The stretching vibrational mode of the water molecules in the hydration shell is thus dominant, with a large population involved in SRS generation, and then the superior SRS performance appears. Moreover, when high concentrations of NaCl are dissolved, a large fraction of the water molecules form hydration shells around Cl^-. The reduced number of remanent water molecules is unfavorable for forming larger water clusters. This is the reason why larger water clusters with strong hydrogen bonds are destroyed by the dissolution of NaCl.

Raising the NaCl concentration leads the shape and the peak of the SRS to shift to a higher wave number, as shown in Figs. 4(a) and 4(c)–4(f). This implies that the interaction between the ions and water in the hydration shells is weakened. This is due to the varying distribution of electric potential around Cl^- associated with varying concentrations. At lower concentrations, the Cl^- and Na^+ ions are far apart from each other, and the water molecules in the hydration shells are arranged around Cl^- ions. The electric potential U_{Cl^-} generated by a Cl^- ion with an electric charge e can be expressed as

$$U_{Cl^-} = \frac{1}{4\pi\varepsilon_0}\frac{e}{r}, \tag{3}$$

where ϵ_0 is the permittivity of the vacuum and r is the distance from the ion. The equipotential surfaces can be seen in Fig. 5.

With an increasing concentration of NaCl, the Cl^- ions tend to combine with Na^+ ions to form ion pairs [67]. When Cl^- and Na^+ ions form an ion pair, the electric potential U_{pair} can be expressed as

$$U_{\text{pair}} = \frac{1}{4\pi\varepsilon_0}\frac{\mathbf{p}\cdot\hat{\mathbf{r}}}{r^2}, \tag{4}$$

where $\mathbf{p}$ is the electric dipole moment of the electric dipole consisting of the Cl^- and Na^+ ions, and $\mathbf{r}$ is the vector from the midpoint of the electric dipole. The equipotential surfaces are plotted in Fig. 5. Compared with a single Cl^- ion, the electric potential of the dipole is inhomogeneous, and the electric potential U at the outer rim of the Cl^- is smaller. With increasing solute concentration, the Cl^- and Na^+ ions tend to remain closer together. The gradient of the electric potential U at the outer rim of Cl^- then diminishes, and the water molecules demonstrate a tendency to be subject to a weaker electric field.

A polar H_2O molecule moving to the outer edge of the Cl^- hydration shell accumulates a potential energy E_P that can be calculated using

$$E_P = \delta(V_{\text{O}} - V_{\text{H}}). \tag{5}$$

Here, δ is the quantity of positive or negative charge on the atoms. V_{O} and V_{H} represent the electric potentials of the O and H atoms, respectively, in the water molecule. It is obvious that the potential energy E_P of water molecules in the hydration shells decreases with increasing solute concentration. The Raman shift then undergoes a redshift. Compared with differential Raman spectroscopy and Raman ratio spectra [35,68], the SRS spectra can probe the O—H stretching vibration frequency and its dependence on concentration directly.

V. CONCLUSION

The SRS properties of water and NaCl solutions are compared in this paper. Owing to the formation of hydration shells when NaCl is by dissolved in water, the SRS threshold can be reduced and the Raman gain can be improved. NaCl solutions that can generate a narrowband SRS laser are more favorable for high-energy optical frequency conversion without being damaged. On the other hand, it is found that the SRS spectrum can provide different insights into liquid structure compared with the spontaneous-Raman-scattering spectrum. The spontaneous-Raman-scattering spectrum is broadband and the corresponding structural analysis is approximate, which makes the assignment of spectral lines difficult, while the distinct peaks in the SRS spectrum can provide more direct evidence about the internal structure of a liquid. Using the SRS spectrum, liquid water is proved to be an assemblage of different clusters that can be identified and quantified. In NaCl solutions, large water clusters with strong hydrogen bonds are destroyed, and hydration shells are formed. The stretching vibration mode of the water in the hydration shell around Cl^- is identified directly, and a structural change in the hydration shell with an increase in NaCl concentration is revealed by a redshift of the SRS peak. These results will be of great significance to further research into the structure and structure-property relationships of water and solutions. Moreover, SRS spectra can be applied to investigate the structure of other liquid compounds and solutions of different concentrations.

ACKNOWLEDGMENTS

This work is supported by the Natural Science Foundation of Shandong Province, China (Grant No. ZR2017MF031), the Open Foundation of the Key Laboratory of Environmental Optics and Technology, Chinese Academy of Sciences (Grant No. 2005DP173065-2018-01), the Program for Outstanding Ph.D. Candidates of Shandong University, the Basic Research and Free Exploration Project of Shenzhen City (Grant No. JCYJ20180305164316517), and the National Natural Science Foundation of China (Grant No. 61975096).

[1] P. Ball, Water as an active constituent in cell biology, Chem. Rev. **108**, 74 (2008).

[2] J. D. Batchelor, A. Olteanu, A. Tripathy, and G. J. Pielak, Impact of protein denaturants and stabilizers on water structure, J. Am. Chem. Soc. **126**, 1958 (2004).

[3] A. Nilsson and L. G. Pettersson, The structural origin of anomalous properties of liquid water, Nat. Commun. **6**, 8998 (2015).

[4] H. D. B. Jenkins and Y. Marcus, Viscosity B-coefficients of ions in solution, Chem. Rev. **95**, 2695 (1995).

[5] M. Kropman and H. Bakker, Dynamics of water molecules in aqueous solvation shells, Science **291**, 2118 (2001).

[6] Z. Sun, L. Zheng, M. Chen, M. L. Klein, F. Paesani, and X. Wu, Electron-hole Theory of the Effect of Quantum Nuclei on the X-ray Absorption Spectra of Liquid Water, Phys. Rev. Lett. **121**, 137401 (2018).

[7] T. R. Prisk, C. Hoffmann, A. I. Kolesnikov, E. Mamontov, A. A. Podlesnyak, X. Wang, P. R. C. Kent, and L. M. Anovitz, Fast Rotational Diffusion of Water Molecules in a 2D Hydrogen Bond Network at Cryogenic Temperatures, Phys. Rev. Lett. **120**, 196001 (2018).

[8] K. H. Kim, H. Pathak, A. Spah, F. Perakis, D. Mariedahl, J. A. Sellberg, T. Katayama, Y. Harada, H. Ogasawara, L. G. M. Pettersson, and A. Nilsson, Temperature-independent Nuclear Quantum Effects on the Structure of Water, Phys. Rev. Lett. **119**, 075502 (2017).

[9] S. Obst and H. Bradaczek, Molecular dynamics study of the structure and dynamics of the hydration shell of alkaline and alkaline-earth metal cations, J. Phys. Chem. **100**, 15677 (1996).

[10] A. M. Saitta and F. Datchi, Structure and phase diagram of high-density water: The role of interstitial molecules, Phys. Rev. E **67**, 020201 (2003).

[11] A. Tongraar, K. R. Liedl, and B. M. Rode, Born-Oppenheimer ab initio QM/MM dynamics simulations of Na^+ and K^+ in water: From structure making to structure breaking effects, J. Phys. Chem. A **102**, 10340 (1998).

[12] B. Hribar, N. T. Southall, V. Vlachy, and K. A. Dill, How ions affect the structure of water, J. Am. Chem. Soc. **124**, 12302 (2002).

[13] E. T. Nibbering and T. Elsaesser, Ultrafast vibrational dynamics of hydrogen bonds in the condensed phase, Chem. Rev. **104**, 1887 (2004).

[14] E. Brini, C. J. Fennell, M. Fernandez-Serra, B. Hribar-Lee, M. Lukšič, and K. A. Dill, How water's properties are encoded in its molecular structure and energies, Chem. Rev. **117**, 12385 (2017).

[15] Y. Marcus, Effect of ions on the structure of water: Structure making and breaking, Chem. Rev. **109**, 1346 (2009).

[16] F. Franks, *Water: a Comprehensive Treatise* (Plenum Press, New York, 1972). Vol. 3.

[17] A. W. Omta, M. F. Kropman, S. Woutersen, and H. J. Bakker, Negligible effect of ions on the hydrogen-bond structure in liquid water, Science **301**, 347 (2003).

[18] J. Duboisset and P. F. Brevet, Salt-induced Long-to-Short Range Orientational Transition in Water, Phys. Rev. Lett. **120**, 263001 (2018).

[19] J. Peng, D. Cao, Z. He, J. Guo, P. Hapala, R. Ma, B. Cheng, J. Chen, W. Xie, X. Li, P. Jelínek, L. Xu, Y. Gao, E. Wang, and Y. Jiang, The effect of hydration number on the interfacial transport of sodium ions, Nature **557**, 701 (2018).

[20] C. Goy, M. A. C. Potenza, S. Dedera, M. Tomut, E. Guillerm, A. Kalinin, K. O. Voss, A. Schottelius, N. Petridis, A. Prosvetov, G. Tejeda, J. M. Fernandez, C. Trautmann, F. Caupin, U. Glasmacher, and R. E. Grisenti, Shrinking of Rapidly Evaporating Water Microdroplets Reveals Their Extreme Supercooling, Phys. Rev. Lett. **120**, 015501 (2018).

[21] D. M. Carey and G. M. Korenowski, Measurement of the Raman spectrum of liquid water, J. Phys. Chem. **108**, 2669 (1998).

[22] T. Okada, K. Komatsu, T. Kawamoto, T. Yamanaka, and H. Kagi, Pressure response of Raman spectra of water and its implication to the change in hydrogen bond interaction, Spectrochim. Acta, Part A **61**, 2423 (2005).

[23] Y. Amo and Y. Tominaga, Dynamical structure of water in aqueous solutions of LiCl, NaCl, and KCl by low-frequency Raman scattering: Comparison between the multiple random telegraph model and Cole-Cole relaxation, Phys. Rev. E **58**, 7553 (1998).

[24] A. W. Omta, M. F. Kropman, S. Woutersen, and H. J. Bakker, Influence of ions on the hydrogen-bond structure in liquid water, J. Phys. Chem. **119**, 12457 (2003).

[25] J. D. Smith, R. J. Saykally, and P. L. Geissler, The effects of dissolved halide anions on hydrogen bonding in liquid water, J. Am. Chem. Soc. **129**, 13847 (2007).

[26] V. G. Savitski, S. Reilly, and A. J. Kemp, Steady-state Raman gain in diamond as a function of pump wavelength, IEEE J. Quantum Electron. **49**, 218 (2013).

[27] H. M. Pask, The design and operation of solid-state Raman lasers, Prog. Quantum Electron. **27**, 3 (2003).

[28] R. C. Prince, R. R. Frontiera, and E. O. Potma, Stimulated Raman scattering: From bulk to nano, Chem. Rev. **117**, 5070 (2016).

[29] T. Li, F. Li, Z. Li, C. Sun, J. Tong, W. Fang, and Z. Men, Influence of strong and weak hydrogen bonds in ices on stimulated Raman scattering, Opt. Lett. **41**, 1297 (2016).

[30] M. Helle, T. Jones, J. Peñano, D. Kaganovich, and A. Ting, Formation and propagation of meter-scale laser filaments in water, Appl. Phys. Lett. **103**, 121101 (2013).

[31] O. T. Ehrler and D. M. Neumark, Dynamics of electron solvation in molecular clusters, Acc. Chem. Res. **42**, 769 (2009).

[32] Z. Men, W. Fang, Z. Li, C. Sun, Z. Li, and X. Wang, Hydrated-electron resonance enhancement O–H stretching

vibration of water hexamer at air–water interface, Opt. Lett. **40**, 1434 (2015).
[33] H. Yuan, B. Gai, J. Liu, J. Guo, H. Li, S. Hu, L. Deng, Y. Jin, and F. Sang, Phase-interfacial stimulated Raman scattering generated in strongly pumped water, Opt. Lett. **41**, 3335 (2016).
[34] H. Yui, Y. Yoneda, T. Kitamori, and T. Sawada, Spectroscopic Analysis of Stimulated Raman Scattering in the Early Stage of Laser-Induced Breakdown in Water, Phys. Rev. Lett. **82**, 4110 (1999).
[35] Y. Gong, Y. Zhou, H. Wu, D. Wu, Y. Huang, and C. Q. Sun, Raman spectroscopy of alkali halide hydration: Hydrogen bond relaxation and polarization, J. Raman Spectrosc. **47**, 1351 (2016).
[36] P. Černý, H. Jelínková, P. G. Zverev, and T. T. Basiev, Solid state lasers with Raman frequency conversion, Prog. Quantum Electron. **28**, 113 (2004).
[37] M. Hippler, Cavity-enhanced Raman spectroscopy of natural gas with optical feedback cw-diode lasers, Anal. Chem. **87**, 7803 (2015).
[38] Y. Ganot and I. Bar, Efficient frequency conversion by stimulated Raman scattering in a sodium nitrate aqueous solution, Appl. Phys. Lett. **107**, 131108 (2015).
[39] Y. Ganot, S. Shrenkel, B. D. Barmashenko, and I. Bar, Enhanced stimulated Raman scattering in temperature controlled liquid water, Appl. Phys. Lett. **105**, 061107 (2014).
[40] V. R. Kumar and P. P. Kiran, Onset of ice VII phase of liquid water: Role of filamentation in stimulated Raman scattering, Opt. Lett. **40**, 2802 (2015).
[41] H. Yui and T. Sawada, Interaction of Excess Electrons with Water Molecules at the Early Stage of Laser-Induced Plasma Generation in Water, Phys. Rev. Lett. **85**, 3512 (2000).
[42] D. Liu, J. Shi, M. Ouyang, X. Chen, J. Liu, and X. He, Pumping effect of stimulated Brillouin scattering on stimulated Raman scattering in water, Phys. Rev. A **80**, 033808 (2009).
[43] See the Supplemental Material at http://link.aps.org/supplemental/10.1103/PhysRevApplied.13.024030, which includes Refs. [31,36,39,40,44–52], for details of the spontaneous Raman scattering (Section I), the first Stokes spectral line near the pump threshold (Section II), and the mechanism of SRS generation (Section III).
[44] G. Herzberg, *Molecular Spectra and Molecular Structure* (Read Books Ltd, Princeton, 2013), Vol. 1.
[45] V. Gorelik, A. Vodchits, and V. Orlovich, Multifrequency stimulated Raman scattering in light and heavy water, J. Russ. Laser Res. **36**, 562 (2015).
[46] Q. Sun, The Raman OH stretching bands of liquid water, Vib. Spectrosc. **51**, 213 (2009).
[47] H. Zhu, Y. Li, S. Vdović, S. Long, G. He, and Q. Guo, Femtosecond coherent anti-Stokes Raman scattering spectroscopy of hydrogen bonded structure in water and aqueous solutions, Spectrochim. Acta, Part A **151**, 262 (2015).
[48] D. Long, *The Raman Effect: A Unified Treatment of the Theory of Raman Scattering by Molecules* (John Wiley & Sons, West Sussex, 2002).
[49] D. J. Spence, Spectral effects of stimulated Raman scattering in crystals, Prog. Quantum Electron. **51**, 1 (2017).
[50] J. Auyeung and A. Yariv, Spontaneous and stimulated Raman scattering in long low loss fibers, Quantum Electron. IEEE J. **14**, 347 (1978).
[51] C. C. Wang, Length dependence of stimulated Raman effect in benzene, J. Appl. Phys. **37**, 1943 (1966).
[52] A. D. Papayannis, G. N. Tsikrikas, and A. A. Serafetinides, Generation of UV and VIS laser light by stimulated Raman scattering in H2, D_2, and H2/He using a pulsed Nd: YAG laser at 355nm, Appl. Phys. B: Lasers Opt. **67**, 563 (1998).
[53] N. Tcherniega, A. Sokolovskaia, A. D. Kudriavtseva, R. Barille, and G. Rivoire, Backward stimulated Raman scattering in water, Opt. Commun. **181**, 197 (2000).
[54] J. Teixeira, The physics of liquid water, J. de Physique IV, Colloque C1, supplement au Journal de Physique 11, 3 (1993).
[55] R. W. Boyd, *Nonlinear Optics* (Elsevier, New York, 2003).
[56] V. R. Kumar and P. P. Kiran, Transformation of liquid water to ice VII during propagation of picosecond laser pulses: Effects of wavelength and polarization, JOSA B **33**, 1157 (2016).
[57] W. Kaiser and M. Maier, *Laser Handbook* (North-Holland, Amsterdam, 1972), Vol. 2.
[58] L. De Boni, C. Toro, and F. E. Hernández, Pump polarization-state preservation of picosecond generated white-light supercontinuum, Opt. Express **16**, 957 (2008).
[59] K. Ohno, M. Okimura, N. Akai, and Y. Katsumoto, The effect of cooperative hydrogen bonding on the OH stretching-band shift for water clusters studied by matrix-isolation infrared spectroscopy and density functional theory, Phys. Chem. Chem. Phys. **7**, 3005 (2005).
[60] W. H. Robertson, E. G. Diken, E. A. Price, J. W. Shin, and M. A. Johnson, Spectroscopic determination of the OH^- solvation shell in the OH − (H2O)n clusters, Science **299**, 1367 (2003).
[61] H. Cybulski and J. Sadlej, On the calculations of the vibrational Raman spectra of small water clusters, Chem. Phys. **342**, 163 (2007).
[62] S. Hartweg, B. L. Yoder, G. A. Garcia, L. Nahon, and R. Signorell, Size-resolved Photoelectron Anisotropy of Gas Phase Water Clusters and Predictions for Liquid Water, Phys. Rev. Lett. **118**, 103402 (2017).
[63] M. F. Kropman and H. J. Bakker, Effect of ions on the vibrational relaxation of liquid water, J. Am. Chem. Soc. **126**, 9135 (2004).
[64] G. Walrafen, Raman spectral studies of the effects of perchlorate ion on water structure, J. Phys. Chem. **52**, 4176 (1970).
[65] N. Galamba, Mapping structural perturbations of water in ionic solutions, J. Phys. Chem. B **116**, 5242 (2012).
[66] M. Ahmed, A. K. Singh, J. A. Mondal, and S. K. Sarkar, Water in the hydration shell of halide ions has significantly reduced Fermi resonance and moderately enhanced Raman cross section in the OH stretch regions, J. Phys. Chem. B **117**, 9728 (2013).
[67] A. P. Lyubartsev and A. Laaksonen, Concentration effects in aqueous NaCl solutions. A molecular dynamics simulation, J. Phys. Chem. **100**, 16410 (1996).
[68] Y. Wang, W. Zhu, K. Lin, L. Yuan, X. Zhou, and S. Liu, Ratiometric detection of Raman hydration shell spectra, J. Raman Spectrosc. **47**, 1231 (2016).